Available online at www.sciencedirect.com

SciVerse ScienceDirect

Scripta Materialia 69 (2013) 262–265

Scripta MATERIALIA

www.elsevier.com/locate/scriptamat

Observation of the defect states in individual Co-doped ZnO dilute magnetic semiconducting nanostructures by electron energy-loss spectroscopy

Z.H. Zhang,[a,b,*] H.L. Tao,[a,b] L.L. Pan,[a,b] Lin Gu,[c] M. He,[a,b] B. Song[d] and Q. Li[e]

[a] *School of Materials Science and Engineering, Department of Physics, Dalian Jiaotong University, Dalian 116028, China*
[b] *Key Laboratory for Photonic and Electric Bandgap Materials, Ministry of Education, Harbin Normal University, China*
[c] *Beijing National Laboratory for Condensed Matter Physics, Institute of Physics, Chinese Academy of Sciences, Beijing 100190, China*
[d] *Academy of Fundamental and Interdisciplinary Sciences, Harbin Institute of Technology, Harbin 150080, China*
[e] *Department of Physics, The Chinese University of Hong Kong, Shatin, New Territory, Hong Kong SAR, China*

Received 6 February 2013; revised 15 March 2013; accepted 14 April 2013
Available online 20 April 2013

Defects play a crucial role in room temperature ferromagnetism of dilute magnetic semiconductors. Using valence electron energy-loss spectroscopy (EELS), it was found that the band gap of Co-doped ZnO was smaller than undoped ZnO and some mid-gap states appeared. Using core-loss EELS, the fine structures of the O K-edge exhibit material-specific defect features in the oxygen spectra. The EELS measurements with super high spatial resolution provide unambiguous indications that defects are presented in Co-doped ZnO nanostructures.

Keywords: Defects; Electron energy-loss spectroscopy; Transmission electron microscopy; Dilute magnetic semiconductors

The zinc oxide (ZnO) based dilute magnetic semiconductor (DMS) has attracted intense research interest as a promising candidate for spintronic materials. Extensive studies on the magnetic properties of ZnO-based semiconductors have been reported [1–6]. However, the nature of the magnetic interactions of ZnO-based semiconductors is very controversial and has attracted global interest as a critical point in the current DMS field. Different mechanisms have been proposed to explain the origin of ferromagnetism in transition-metal-doped ZnO [7–9]. Among them, the bound magnetic polaron theory plays a key role in understanding the ferromagnetism observed in ZnO-based semiconductors. Defects introduced into ZnO-based DMS system during sample preparation, including O vacancies [10–12], Zn vacancies [13] and Zn interstitials [14,15], might be responsible for the promotion of ferromagnetism. However, it is very difficult to observe such defects experimentally. Although dozens of articles have mentioned such defects, hardly any of them have provided any direct evidence for the presence of defects in DMS. This is particularly difficult to do in the nanostructured ZnO systems due to the non-uniform characteristic of the nanosamples. Macroscopic measurements must be performed on a large quantity of nanostructures. Also, the observation of a defect at the macroscopic scale does not mean the presence of such a defect in the individual nanostructures.

Defects can impart defects states to the electronic structures of host semiconductors and drive the functionality of the materials. Identifying and positioning these defect states provides an alternative way to show the defect in an ZnO-based DMS system. However, it is apparently not easy to unambiguously depict the defect states experimentally, and particularly positioning them in the electronic structures of individual DMS nanostructures, due to the lack of a spectroscopic probe that possesses both nanometer spatial resolution and chemical resolution. Electron energy-loss spectroscopy (EELS), combined with transmission electron microscopy (TEM), has super high spatial resolution and can be used to study individual nanostructures. However,

* Corresponding author at: School of Materials Science and Engineering, Department of Physics, Dalian Jiaotong University, Dalian 116028, China. Tel.: +86 411 84105700; fax: +86 411 84109417; e-mail: zhzhang@djtu.edu.cn

1359-6462/$ - see front matter © 2013 Acta Materialia Inc. Published by Elsevier Ltd. All rights reserved.
http://dx.doi.org/10.1016/j.scriptamat.2013.04.016

in general, the energy resolution of EELS is limited to ~0.8 eV, which is too low to detect the presence of a defect state in an individual nanostructure. Remarkably, in the past two years, the energy resolution of EELS has improved greatly (about 0.2–0.3 eV) as a result of the application of a monochromator. Valence EELS possesses near-optical energy resolution and can be used to reproduce the bandgap of semiconductors reliably. The fine structures of core-loss EELS provide detailed environmental information about localized atoms. Here, we employed an EELS-related technique to investigate the defect states in individual Co-doped ZnO nanostructures. The measured valence EELS and the O K near-edge fine structure are found to exhibit different spectral features between Co-doped ZnO and undoped ZnO. The presence of defect states in individual Co-doped ZnO DMS nanostructures is identified experimentally, providing evidence that defects play a crucial role in the room-temperature ferromagnetism of nanostructured DMS systems.

The studied Co-doped ZnO nanoparticles were synthesized by a simple solvothermal technique [16,17]. The samples demonstrated robust high-temperature (300 K) ferromagnetic behavior, which has been proved to be an intrinsic property of the individual nanostructures using an atom location by channeling enhanced microanalysis, EELS and electron magnetic chiral dichroism method [16]. The sample with a Co concentration of ~5.6% was chosen for the EELS measurement as it provided the best signal-to-noise ratio. The microstructures of the samples were examined using various TEM-related techniques. Spherical aberration-corrected scanning transmission electron microscopy (STEM) was performed using a JEOL 2100F transmission electron microscope equipped with a CEOS (Heidelberg, Germany) probe aberration corrector. The EELS experiments were performed using a post-column Gatan Imaging Filter system attached to a Titan microscope (Titan G2 60-300) with energy resolutions of ~0.3 and 1.0 eV for valence and core-loss EELS, respectively.

The typical morphologies of the Co-doped ZnO nanostructures are shown in Figure 1a. Selected area electron diffraction (SAED) patterns taken from individual nanostructures reveal their single crystalline hexagonal structure, which is further confirmed by the corresponding high-resolution images (not shown here). Some streak-like lines are observed in the SAED patterns, indicating the possible presence of defects in the studied specimen. The local chemical compositions of the samples are characterized by energy-dispersive X-ray spectroscopy (EDS) using a ~1 nm electron probe. In each of the samples, EDS was performed at several different locations with similar chemical compositions (Zn, O, Co) identified, suggesting that the dopant ions were distributed uniformly. No clustering of the Co is observed in the samples and the Co concentration is estimated as ~5.6%. Spherical aberration-corrected STEM has showed its potential for mapping point defects, which is capable of spatial sub-angstrom resolution [18]. Therefore, to visualize the defect in the system, the aberration-corrected STEM technique was employed. Figure 1c shows the high-angle annular dark-field (HAADF) image and Figure 1d shows the

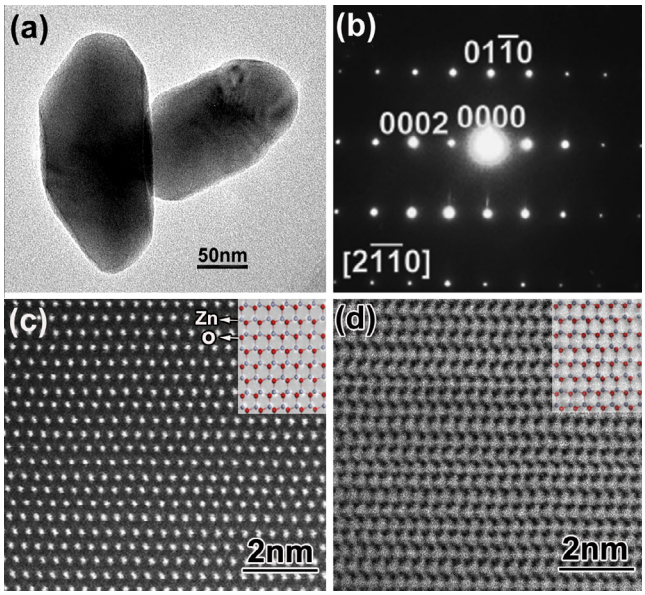

Figure 1. (a) Low-magnification TEM images of the Co-doped ZnO sample; (b) the corresponding selected area electron diffraction pattern; (c, d) HAADF and ABF images taken from the Co-doped ZnO nanostructure. The insets in (c) and (d) are the atom arrangements of Co-doped ZnO along the [2-1-10] direction.

annular bright-field (ABF) image along the [2-1-10] direction recorded from the nanostructures. Note that the contrast of the HAADF image exhibits a $Z^{1.7}$ dependence, as compared with a $Z^{1/3}$ for the ABF image with respect to the atomic number Z [19,20]. The atomic columns shown in Figure 1c and d have direct correspondence with the atoms in the perfect lattice structure of Co-doped ZnO (shown as insets in Fig. 1c and d). The Zn and O columns can be identified clearly based on the contrast, while Zn ($Z = 30$) and Co ($Z = 27$) atoms cannot be identified because of their similar atomic numbers and the low doping concentration of Co. No second phases or defect structures, such as O vacancies or Zn interstitials, were observed in the HAADF and ABF images, suggesting that the concentration of the defects may be below the lowest detection limit of the techniques.

The raw valence EELS spectrum recorded from the individual Co-doped ZnO nanostructures is shown as an inset in Figure 2a and the loss function obtained from the raw spectrum by removing the plural scattering using a direct deconvolution method [21] is shown in Figure 2a. For comparison, the raw valence EELS spectrum acquired from the undoped ZnO is shown as an inset in Figure 2b and the corresponding loss function is shown in Figure 2b. The three Co dopant characteristic states (marked by "*") identified by Wang et al. [17] are clearly seen in the present spectrum (Fig. 2a). (Note that Wang et al. cut their EELS spectra before 5 eV, so the spectra in this range are our focus on in the discussion below.)

There are two obvious differences when comparing the loss functions of Co-doped ZnO with those of undoped ZnO. First, the band gap of the Co-doped ZnO is slightly smaller than that of undoped ZnO, as shown

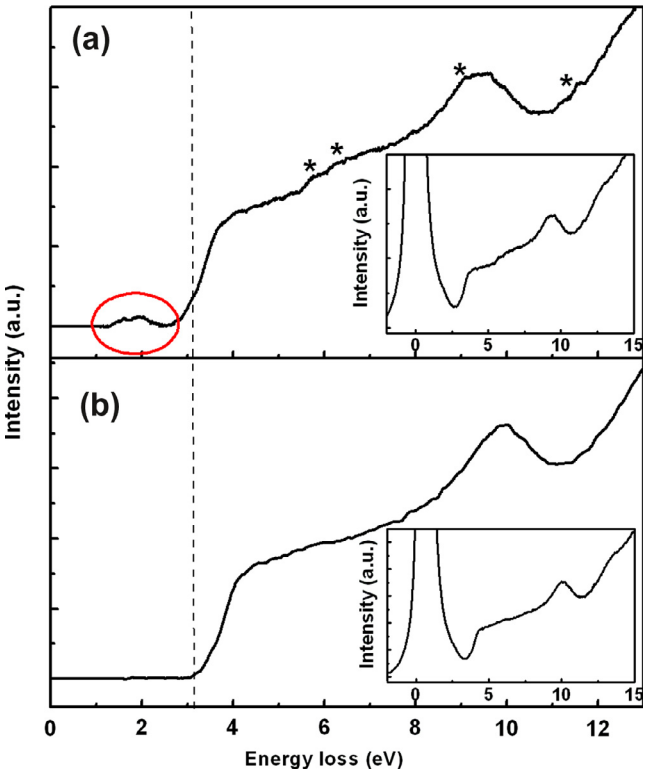

Figure 2. The loss functions of (a) Co-doped ZnO and (b) undoped ZnO. The insets show the corresponding raw valence EELS recorded from Co-doped ZnO and undoped ZnO.

by the valley at ~3 eV (a dashed line is drawn as a visual guide), which is confirmed by the results of Wang et al. (see figure S3d–f in the supporting information to Ref. [17]). Second, an obvious midgap band (indicated by a red circle in Fig. 2a) with an excitation energy of 1.3–2.5 eV appears in the Co-doped ZnO nanostructures but is absent in the undoped ZnO. The different spectral features reflect different electronic structures in the Co-doped ZnO and undoped ZnO samples. A decrease in the band gap of ~0.1 eV has been observed by optical transmission in Co-doped ZnO films [22], thus the smaller band gap is partially due to the doping effect. On the other hand, many theoretical studies on the defect states in Co-doped ZnO [23,24] have reported that the donor defect states overlap with the bottom of the conduction band and therefore diminish the band gap of Co-doped ZnO. The O vacancy or vacancy complex can induce additional donor states within the gap [23,24]. Comparing the theoretical and the experimental results, the donor defect states within the gap are the origination of the midgap states observed in our valence EELS spectrum. Thus, the two characters (the smaller band gap and the midgap states) in valence EELS provide evidence of the presence of defects in the Co-doped ZnO nanostructures studied.

The core loss O K-edge spectrum recorded from the Co-doped ZnO sample is shown in Figure 3a and the O K-edge spectrum acquired from the undoped ZnO is shown in Figure 3b. For comparison, the spectra are normalized to the same peak height. The features between 530 and 580 eV of the undoped ZnO (labeled *a*–*c*) are

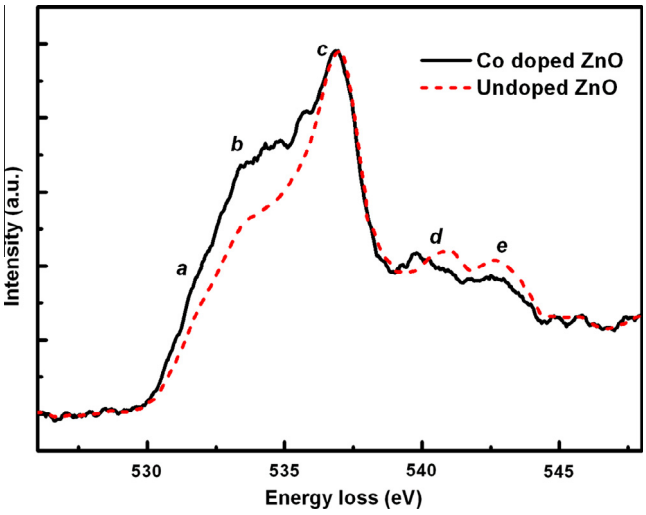

Figure 3. The fine structures of O K-edge for Co-doped ZnO (black solid line) and undoped ZnO (red dashed line), respectively. (For interpretation of the references to colour in this figure legend, the reader is referred to the web version of this article.)

assigned to O2*p*–Zn4*s* hybridized states, while the features *d* and *e* arise from O2*p* states hybridized with Zn4*p* states [22,10]. In the case of Co-doped ZnO, the O K-edge shows more spectral weight close to the conduction band minimum (feature *a*), and the spectral weight at 533.5 eV (feature *b*) is also higher. Oxygen vacancy results in the reduction and broadening of feature *b*, while the Co interstitials do not change this feature but enhance the *a* fine structures [22,10]. Therefore, the different O K-edges of Co-doped ZnO and undoped ZnO seem to be caused by the oxygen vacancy defects or the Co interstitials. On the other hand, a shift in the onset energy is observed when comparing the O K-edge of Co-doped ZnO with that of undoped ZnO. Note that the observed decrease in the band gap of ~0.2 eV was been measured by valence EELS (Fig. 2) and the shift in the onset of the oxygen K edge has been confirmed by X-ray absorption spectroscopy experiments [22] (proposed to be due to the presence of oxygen vacancies). Thus the core-loss O K-edge spectroscopic measurements on Co-doped ZnO exhibit material-specific defect features, which is consistent with the conclusion obtained from the valence EELS measurements. There was no change in the studied specimen after a long period of radiation with our incident electron beam, so the pre-peak observed in Ref. [25] as a result of radiation damage was not observed in our specimen.

In conclusion, we studied the possible existence of defects in individual Co-doped ZnO nanostructures. Using a spherical aberration-corrected STEM technique, no secondary phases and no defect structures were observed in individual Co-doped ZnO nanostructures. Using valence EELS, the band gap of Co-doped ZnO was found to be smaller than undoped ZnO and some midgap states appeared, which were identified as resulting from the presence of defect states in Co-doped ZnO. Using core-loss EELS, the O K-edge characters of Co-doped ZnO show material-specific defect features in the oxygen spectra. The results presented here provide

unambiguous evidence that defects are present in individual Co-doped ZnO nanostructures and may play a crucial role in room-temperature ferromagnetism.

This work was sponsored by National Natural Science Foundation of China under Grant Nos. 50902014, 50902037 and 51002017. Q.L. acknowledges financial support from RGC of HKSAR under Grant No. 402007. Supported by the Open Project Program of Key Laboratory for Photonic and Electric Bandgap Materials, Ministry of Education, Harbin Normal University, China.

[1] H. Lee, S. Jeong, C. Cho, C. Park, Appl. Phys. Lett. 81 (2002) 4020.
[2] K. Sato, H. Katayama-Yoshida, Jpn. J. Appl. Phys. 40 (2001) L334.
[3] A. Barla, G. Schmerber, E. Beaurepaire, A. Dinia, H. Bieber, S. Colis, F. Scheurer, J.-P. Kappler, P. Imperia, F. Nolting, F. Wilhelm, A. Rogalev, D. Müller, J.J. Grob, Phys. Rev. B 76 (2007) 125201.
[4] G. Lawes, A.S. Risbud, A.P. Ramirez, R. Seshadri, Phys. Rev. B 71 (2005) 045201.
[5] T. Dietl, Nat. Mater. 9 (2010) 965.
[6] J. Coey, M. Venkatesan, C. Fitzgerald, Nat. Mater. 4 (2005) 173.
[7] T. Story, R.R. Galazka, R.B. Frankel, P.A. Wolff, Phys. Rev. Lett. 56 (1986) 777.
[8] K.R. Kittilstved, W.K. Liu, D.R. Gamelin, Nat. Mater. 5 (2006) 291.
[9] J.M.D. Coey, M. Venkatesan, C.B. Fitzgerald, Nat. Mater. 4 (2005) 173.
[10] G.S. Chang, E.Z. Kurmaev, D.W. Boukhvalov, L.D. Finkelstein, S. Colis, T.M. Pedersen, A. Moewes, A. Dinia, Phys. Rev. B 75 (2007) 195215.
[11] H.S. Hsu, J.C.A. Huang, Appl. Phys. Lett. 88 (2006) 242507.
[12] W.S. Yan, Q.H. Jiang, Z.H. Sun, T. Yao, F.C. Hu, S.Q. Wei, J. Appl. Phys. 108 (2010) 013901.
[13] C.H. Patterson, Phys. Rev. B 74 (2006) 144432.
[14] T.F. Shi, Z.G. Xiao, Z.J. Yin, X.H. Li, Y.Q. Wang, H.T. He, J.N. Wang, W.S. Yan, S.Q. Wei, Appl. Phys. Lett. 96 (2010) 211905.
[15] C.D. Pemmaraju, R. Hanafin, T. Archer, H.B. Braun, S. Sanvito, Phys. Rev. B 78 (2008) 054428.
[16] Z.H. Zhang, X.F. Wang, J.B. Xu, S. Muller, C. Ronning, Q. Li, Nat. Nano. 4 (2009) 523.
[17] X.F. Wang, F.Q. Song, Q. Chen, T.Y. Wang, J.L. Wang, P. Liu, M.R. Shen, J.G. Wan, G.H. Wang, J.B. Xu, J. Am. Chem. Soc. 132 (2010) 6492.
[18] L. Fitting, S. Thiel, A. Schmehl, J. Mannhart, D.A. Muller, Ultramicroscopy 106 (2006) 1053.
[19] S.D. Findlay, N. Shibata, H. Sawada, E. Okunishi, Y. Kondo, T. Yamamoto, Y. Ikuhara, Appl. Phys. Lett. 95 (2009) 191913.
[20] S.D. Findlay, N. Shibata, H. Sawada, E. Okunishi, Y. Kondo, T. Yamamoto, Y. Ikuhara, Ultramicroscopy 110 (2010) 903.
[21] R.F. Egerton, Electron Energy Loss Spectroscopy in the Electron Microscope, Plenum Press, New York, 1996.
[22] S. Krishnamurthy, C. McGuinness, L.S. Dorneles, M. Venkatesan, J.M.D. Coey, J.G. Lunney, C.H. Patterson, K.E. Smith, T. Learmonth, P.A. Glans, T. Schmitt, J.H. Guo, J. Appl. Phys. 99 (2006) 08M111.
[23] S.J. Hu, S.S. Yan, M.W. Zhao, X.L. Lin, X.X. Yao, C. Han, Y.F. Tian, Y.X. Chen, G.L. Liu, L.M. Mei, Scripta Mater. 64 (2011) 864.
[24] C.D. Pemmaraju, R. Hanafin, T. Archer, H.B. Braun, S. Sanvito, Phys. Rev. B 78 (2008) 054428.
[25] Q.M. Ramasse, A.P. Kuprin, M. Chi, T.C. Kaspar, S.A. Chambers, N.D. Browning, Microsc. Microanal. 15 (suppl. 2) (2009) 437.